EDGEWOOD CHEMICAL BIOLOGICAL CENTER
U.S. ARMY RESEARCH, DEVELOPMENT AND ENGINEERING COMMAND
Aberdeen Proving Ground, MD 21010-5424

ECBC-TR-1470

REDUCING FALSE ALARMS IN ION MOBILITY SPECTROMETRY DETECTORS: DETERMINATION OF ACCURATE AND PRECISE REDUCED MOBILITY VALUES

Brian C. Hauck
William F. Siems
Herbert H. Hill, Jr.

WASHINGTON STATE UNIVERSITY
Pullman, WA 99164-4630

Vincent M. McHugh

RESEARCH AND TECHNOLOGY DIRECTORATE

Charles S. Harden

LEIDOS
Abingdon, MD 21009-1261

November 2017

U.S. ARMY RDECOM

Disclaimer

The findings in this report are not to be construed as an official Department of the Army position unless so designated by other authorizing documents.

REPORT DOCUMENTATION PAGE

Form Approved
OMB No. 0704-0188

1. REPORT DATE *(DD-MM-YYYY)*	**2. REPORT TYPE**	**3. DATES COVERED** *(From - To)*
XX-11-2017	Final	Sep 2012 – Sept 2016

4. TITLE AND SUBTITLE
Reducing False Alarms in Ion Mobility Spectrometry Detectors: Determination of Accurate and Precise Reduced Mobility Values

5a. CONTRACT NUMBER

5b. GRANT NUMBER
W911NF-12-1-0575

5c. PROGRAM ELEMENT NUMBER

6. AUTHOR(S)
*Hauck, Brian C.; Siems, William F.; Hill, Herbert H., Jr. (WSU); McHugh, Vincent M. (ECBC); **Harden, Charles S. (Leidos)

5d. PROJECT NUMBER

5e. TASK NUMBER

5f. WORK UNIT NUMBER

7. PERFORMING ORGANIZATION NAME(S) AND ADDRESS(ES)
Washington State University, Department of Chemistry, Pullman, WA 99164-4630
Director, ECBC, ATTN: RDCB-DRI-D, APG, MD 21010-5424
Leidos, 3465 Box Hill Corporate Center Dr., Abingdon, MD 21009-1261

8. PERFORMING ORGANIZATION REPORT NUMBER
ECBC-TR-1470

9. SPONSORING / MONITORING AGENCY NAME(S) AND ADDRESS(ES)
U.S. Army Research Office, P.O. Box 12211, Research Triangle Park, NC 27709-2211

10. SPONSOR/MONITOR'S ACRONYM(S)
ARO

11. SPONSOR/MONITOR'S REPORT NUMBER(S)

12. DISTRIBUTION / AVAILABILITY STATEMENT
Approved for public release: distribution unlimited.

13. SUPPLEMENTARY NOTES
*Brian C. Hauck is no longer employed by WSU.
** Charles S. Harden is no longer employed by Leidos.

14. ABSTRACT:
Ion mobility spectrometry (IMS) is a widely used analytical technique for field detection of chemical warfare agents (CWAs), narcotics, and explosives. Detection is based on the reduced mobility (K_0) of the compound of interest (COI). The detection windows for COIs have historically been as small as ±2% of the predicted COI K_0 value ($K_{0\,\mathrm{COI}}$), which resulted in false-positive alarms when an interferent appeared within these wide detection windows. Accurate K_0 values that are an order of magnitude better than the values given in literature lower the propagation of error when they are used to predict the drift time of an ion and reduce the width of the detection windows. An IMS instrument was constructed and interfaced with an existing time-of-flight mass spectrometer, and select $K_{0\,\mathrm{COI}}$ values were measured as a function of multiple instrumental parameters. This initial database of accurate $K_{0\,\mathrm{COI}}$ values will be expanded in the future to include additional COIs, namely CWAs (toxic chemicals) and explosives. The database of accurate K_0 values will be used to calibrate IMS-based field instruments and reduce their rates of false-positive alarms without increasing their false-negative responses or modifying hardware.

15. SUBJECT TERMS
Ion mobility spectrometry (IMS) Reduced mobility (K_0) False alarms Explosives
Chemical warfare agent (CWA)

16. SECURITY CLASSIFICATION OF:			**17. LIMITATION OF ABSTRACT**	**18. NUMBER OF PAGES**	**19a. NAME OF RESPONSIBLE PERSON**
a. REPORT	**b. ABSTRACT**	**c. THIS PAGE**			Renu B. Rastogi
U	U	U	UU	44	**19b. TELEPHONE NUMBER** *(include area code)* (410) 436-7545

Blank

EXECUTIVE SUMMARY

Ion mobility spectrometry (IMS) is a gas-phase separation technique used by the U.S. Military and other organizations for explosives and chemical warfare agent (CWA) detection. IMS-based field detection instruments are subjected to false-positive alarms because of wide detection windows that result from inaccurate reduced mobility (K_0) values of ions. The overall goals of our work were two-fold:

- Construct an accurate IMS instrument capable of measuring K_0 values to an accuracy of ±0.2% (±0.002 $cm^2V^{-1}s^{-1}$) or better, which would be an order of magnitude better than existing capabilities; and
- Make accurate and precise experimental measurements of K_0 values for select target chemicals.

The objectives of the experimental work detailed in this report were to

- construct and hermetically seal an accurate IMS instrument;
- introduce, ionize, and analyze the following compounds by IMS:
  - ammonia reactant ion (positive ion mode active);
  - DMMP: dimethyl methylphosphonate (positive ion mode active);
  - TNT: 2,4,6-trinitrotoluene (negative ion mode active);
  - RDX: 1,3,5-trinitroperhydro-1,3,5-triazine (negative ion mode active);
  - PETN: 2,2-bis[(nitrooxy)methyl]propane-1,3-diyl dinitrate (negative ion mode active); and
- obtain K_0 values for each of the above compounds at varying electric field strengths, drift gas water vapor concentration, and temperatures.

The results of the positive-mode study were as follows:

- The K_0 values of the DMMP monomer and ammonia reactant ion increased with increasing temperature;
- The K_0 values of the DMMP monomer and ammonia reactant ion decreased with increasing drift gas water content;
- The K_0 value of the DMMP dimer did not significantly change with changing temperature or drift gas water content; and
- The K_0 values of all the ions that were studied decreased with increasing electric field strength.

The results of the negative mode study were as follows

- The K_0 values of all the ions that were studied increased with increasing temperature;
- The K_0 values of all the ions that were studied decreased with increasing drift gas water content; and
- The K_0 values of all the ions that were studied decreased with increasing electric field strength.

The impact of the work will be to

- create an initial database of accurate K_0 values for the compounds of interest that were studied,
- enable the selection and evaluation of an appropriate mobility reference standard to calibrate IMS-based field instruments in real time,
- reduce the false-positive alarm rates of IMS-based field instruments without increasing the rates of false-negative responses, and
- make these improvements to IMS-based field instruments using only software changes and without expending resources for hardware changes.

PREFACE

The work described in this report was initially funded by Leidos (Abingdon, MD), as a subcontract under a Task Order contract with the U.S. Army Edgewood Chemical Biological Center (Aberdeen Proving Ground, MD). Funding was then assumed by the U.S. Army Research Office (Research Triangle Park, NC) under grant number W911NF-12-1-0575. The work was started in September 2012 and completed in September 2016.

Acknowledgments

The authors acknowledge the following individuals for their hard work and assistance with the execution of this technical program: Dave Savage, Lauren Frei, Steve Watson, and Fred Schutze of Washington State University's Technical Services Instrument and Electronics shops (Pullman, WA).

Blank

CONTENTS

FIGURES

TABLES

Blank

REDUCING FALSE ALARMS IN ION MOBILITY SPECTROMETRY DETECTORS: DETERMINATION OF ACCURATE AND PRECISE REDUCED MOBILITY VALUES

1. INTRODUCTION

Ion mobility spectrometry (IMS) is the preferred analytical technique in the detection of chemical warfare agents (CWAs), narcotics, and explosives within the realm of national security. Compounds of interest (COIs) are identified by using the reduced mobility (K_0) of an ion, which is calculated by the amount of drift time (t_d) it takes for the ion to drift a known length (L) under a voltage gradient (V) applied across L. The experimental temperature (T) and pressure (P) are normalized to standard temperature and pressure, as shown in eq (1).[1]

$$K_0 = \frac{L^2}{V t_d}\left(\frac{273.15}{T}\right)\left(\frac{P}{760}\right) \quad (1)$$

A field instrument is used to search for a COI, such as an explosive, by predicting the K_0 value of the COI ($K_{0\,COI}$) and establishing a detection window around that predicted K_0 value. The $K_{0\,COI}$ is predicted by using the known K_0 value of a reference standard ($K_{0\,std}$) from the available literature and the measured t_d of the reference standard ($t_{d\,std}$) to determine the instrument factor (C_i), which takes into account the parameters (L, V, T, and P) for the specific instrument being used. The quotient of C_i divided by the measured t_d of the target COI ($t_{d\,COI}$) produces the predicted $K_{0\,COI}$ value, as shown in eq (2).[2–8]

$$\frac{(K_{0\,std})t_{d\,std}}{t_{d\,COI}} = \frac{C_i}{t_{d\,COI}} = K_{0\,COI} \quad (2)$$

Once the $K_{0\,COI}$ has been predicted from C_i and $t_{d\,COI}$, a detection window is set up around the predicted $K_{0\,COI}$ through the propagation of error shown in eq (2). If a K_0 spectral peak falls within the window, it is deemed a true positive response for the COI. The width of the detection window and the error in any predicted $K_{0\,COI}$ has been historically accurate to ±2%.[3,9] Whenever an interferent with a K_0 value within 2% of the predicted $K_{0\,COI}$ falls within the detection window, this results in a false-positive alarm and causes the loss of time and money, as resources are diverted to respond to the alarm. However, these detection windows cannot be arbitrarily decreased because of the risk of excluding a true COI peak from the detection window, which results in a false-negative response.

The only way to reduce the width of detection windows and improve specificity without inadvertently decreasing sensitivity is to increase the accuracy of K_0 values referenced by the field instruments when predicting the $K_{0\,COI}$ value in eq (2). To measure accurate reference $K_{0\,COI}$ values, each of the variables (i.e., L [cm], V [V], t_d [ms], T [K], and P [Torr]) need to be accurately and precisely measured and controlled so that the error that is propagated through the calculation of the K_0 values is reduced. After a database of accurate $K_{0\,COI}$ values that

include mobility reference standards and hazards is created, the values will be referenced by an improved detection algorithm program. This program will be used for real-time calibration of the IMS-based field instruments.

For this work, our objective was to construct an accurate IMS instrument that could be used to measure K_0 values to an accuracy of ±0.2% (±0.002 $cm^2V^{-1}s^{-1}$) or better. After the instrument was completed, select COIs were analyzed, and accurate K_0 values were obtained as a function of temperature, drift gas water content, and electric field. This report details the final results that were obtained for the U.S. Army Edgewood Chemical Biological Center (ECBC) proposal number 62620-CH, agreement number W911NF-12-1-0575, which was conducted under the direction of Dr. Herbert H. Hill, Jr. (Co-Principal Investigator, Washington State University [WSU]; Pullman, WA). The first half of the report details the method used for the construction of the IMS instrument and the equipment and procedures required to accurately and precisely control the five variables within eq (1). These details and other related scientific progresses have been published in open literature.[10–13] The second half of this report consists of the initial database of accurate K_0 values obtained for six ions and analyses of the trends found in the data.

2. SCIENTIFIC PROGRESS AND ACCOMPLISHMENTS

2.1 Error Reduction

The degree of error in calculating K_0 values with the IMS instrument is dependent upon the measured accuracies of the components within the system as they relate to the five variables of eq (**1)**. The potential for error from each of these parameters was minimized by using the highest accuracy components and procedures, thereby reducing each variable's error in measurement and control.

2.1.1 Length (*L*)

The length of the drift tube was defined as the distance between two sets of Bradbury–Nielson (BN) ion gate wires. The length between the BN ion gates was calculated by measuring the sum of three lengths (length of half of each gate and the length of the drift tube between both BN ion gates) at room temperature. The length was measured using a pair of 12 in. calipers from Mitutoyo Instruments (Aurora, IL) that had an error of ±0.0015 in. (±0.0381 mm). All length measurements were corrected for thermal expansion.

2.1.2 Voltage (*V*)

Voltage was supplied to the drift tube by an LS020 reversible 20 kV power supply from Exelis, Inc. (West Springfield, MA). The power supply was capable of a 20 kV maximum output and had a 1 ppm output ripple. The electric field (*E*) within the IMS instrument was set up to be homogenous and adjustable from the first electrode to the inlet of the time-of-flight mass spectrometer (*tof*MS); the *E* terminated at the same potential as the inlet of the *tof*MS. A series of 20 ±1% MΩ resistors (Caddock Electronics Inc.; Riverside, CA) were attached between

electrode rings with pin connectors (Positronic Industries, Inc.; Springfield, MO). A 5 MΩ variable resistor (Newark element14; Chicago, IL) was attached as a potentiometer across the drift gas entry showerhead after the second BN ion gate, and a second series of 5 MΩ variable resistors leading to ground were attached to the end of the resistor chain to establish the electric field. The electric field was set to the desired value by adjusting the voltage applied to the first ring (V_s) and the total resistance of the chain after the potentiometer. Instead of using 20 MΩ resistors, two 10 MΩ resistors (±1%) from Caddock were used across the first BN ion gate and a third 10 MΩ resistor was used leading up to the second BN ion gate reference.

The voltage across the drift space was measured using an 8846A digital multimeter (DMM; Fluke Corporation; Everett, WA). The DMM had an accuracy of ±0.0024% of the measurement plus 0.0005% of the DMM range used. The DMM was coupled with a 10 GΩ high-precision HVP-250 voltage divider (Computer Power Supplies; Tigard, OR), which had an accuracy of ±0.05% over the full measurement. The divider had a ratio of 10,000:1 (measured directly to $1.003 \times 10^{-4} \pm 5 \times 10^{-7}$) and required the DMM to be used in high-input impedance mode when voltage was measured because the resulting input voltage was <1 V.

The power supply had such a low output current that higher resistors were required in the electric field. However, because the 10 GΩ voltage divider had a comparatively high resistance to that of the total resistor chain on the IMS instrument, it offered the current running through the resistor chain an alternate path to ground of near equivalent resistance and drew down the observed voltage measurement when the probe was applied. This necessitated a correction to the measurement obtained from the DMM to determine the "true" voltage at the measurement point using eq (3).

$$V_{\text{true}} = V_{\text{meas}} \left(\frac{IIR + R_{\text{upfld}}}{IIR} \right) \left(\frac{R_{\text{dwnfld}}}{R_{\text{T}}} \right) \left(\frac{1}{PDR} \right) \quad (3)$$

In eq (3), V_{true} is the true value of the voltage applied to the electrode, V_{meas} is the voltage measured directly with the high voltage (HV) probe and DMM, *IIR* is the parallel resistance between the HV probe and the resistor chain downfield (towards ground) from the measurement point, R_{upfld} is the total value of the entire resistor chain upfield (towards the first electrode) from the measurement point, R_{dwnfld} is the value of the resistor chain downfield from the measurement point, R_{T} is the value of the total resistor chain, and *PDR* is the value of the HV probe divider ratio, which was previously stated. The directly measured values of the resistors, as opposed to their nominal values, were used in eq (3). The voltage difference between the first and second BN ion gate reference voltages was used in reduced mobility calculations to correspond with the length measured between the BN ion gate wires.

The closure voltage at both BN ion gates was scaled with the electric field to maintain a homogenous electric field and to have ions pass through identical equipotential lines between the BN ion gate wires for each electric field. To determine the minimum BN ion gate closure voltage, the IMS instrument was operated in manual mode with the first BN ion gate

closed at the lowest field. The BN ion gate closure voltage was slowly increased until no spectra appeared over the course of 20 min. This minimum BN ion gate closure voltage was then scaled for each successive electric field. When one BN ion gate was operated to collect spectra, the other one was connected to the resistor chain using wire and alligator clips to maintain the homogeneity of the electric field. The gate pulse width was maintained at 200 µs for all the t_d measurements at both BN ion gates.

2.1.3 Drift Time (t_d)

The *tof*MS was used to measure the t_d values for all of the ions. Two separate t_d values were recorded: the first t_d measurement was from the first BN ion gate and the second one was from the second BN ion gate. The t_d between the two BN ion gates was determined by taking the difference between the two t_d measurements. The time spent past the second BN ion gate and within the *tof*MS was thereby eliminated. This way, the t_d measurement between the two BN ion gates directly corresponded with the measured length between the two BN ion gates. All K_0 values used t_d measurements obtained in the IMS–MS mode to mass identify all the product ions.

The IMS instrument was also programmed to measure the t_d in IMS standalone mode using a Faraday plate, which was built into its drift gas entry at WSU. When using the Faraday plate, the first BN ion gate was used in the same manner as the IMS–MS mode, and the second gate was used as an aperture grid. Spectra for the Faraday plate were obtained and analyzed using a Labview software program, which was written in-house at WSU.[14]

2.1.4 Temperature (T)

The IMS instrument was heated by two 25.5 cm long heater cartridges (Heatcon, Inc.; Seattle, WA) inserted into the aluminum thermal case. These cartridges were controlled by a pair of CN7823 DIN temperature controllers (Omega; Stamford, CT). These controllers were used to measure the temperature of the thermal case using a pair of resistive temperature devices (RTDs)-850 (Omega) embedded in the thermal case. The temperature controllers had an output accuracy of ±0.1 °C, and the RTDs had a measurement accuracy of ±0.15 °C. The thermal case was insulated by a custom-built insulation sleeve (LCS Isotherm; Frankfurt, Germany).

Preheating the drift gas above the desired temperature before it entered the showerhead reduced the temperature gradient within the drift tube. This compensated for the heat sink behind the IMS instrument created by the *tof*MS. The drift gas was preheated using a heater built in-house at WSU, which consisted of an 8 in. length of 1/8 in. stainless steel tubing wrapped with 3 ft of 90 Ω/ft resistance wire (California Fine Wire Company; Grover Beach, CA) covered in a protective outer sheath. A Variac supplied a constant voltage to the heater through an electrical plug connected to the resistance wire.

The temperature value of the drift gas used in reduced mobility calculations was measured by two T100-250 probes, which had an accuracy of ±0.01 °C, coupled to an F200 precision thermometer (both were from Isotech North America, Inc.; Colchester, VT). Each probe was inserted into the drift space through the two hollow electrode posts in front of each

BN ion gate. Temperature gradients were measured for 24 h at each setting and the averages between the two measurement points were used in the K_0 calculations for each temperature setting. All the average temperatures that were used had a gradient between measurement points of <0.1 ºC associated with them.

2.1.5 Pressure (*P*)

Ambient pressure experiments (approximately 697 Torr for Pullman, WA) used a 230–7420 mercury barometer (NovaLynx Corporation; Grass Valley, CA). The barometer had an accuracy of ±0.2 Torr after it was corrected for temperature and latitude at the measurement site. Sub-ambient pressures could be achieved using a 640A pressure controller (MKS Instruments; Andover, MA) in conjunction with a DS 42 rotary vane vacuum pump (Agilent Technologies, Vacuum Products Division; Lexington, MA). The pressure controller contained a capacitance manometer and had an accuracy of ±0.5%. The counter current drift gas was maintained at 1.00 ± 0.01 L/min with an 1179A digital mass flow controller and 247D four-channel power supply and display (MKS instruments). All the K_0 values were measured at an ambient pressure.

2.2 Construction and Operation of the Accurate IMS Drift Tube

2.2.1 Drift Rings

The drift rings that made up the IMS drift tube were used to establish the voltage gradient and electric field for the ions to follow towards the detector. The drift rings consisted of a ceramic insulator and metal electrode rings. The insulator rings were made out of alumina (99.8%; Al_2O_3), and their dimensions were 60.5 mm inside diameter (i.d.), 69 mm outside diameter (o.d.), and 7 mm wide. The electrode rings were machined from Alloy 46 (National Electronic Alloys; Oakland, NJ), a nickel-iron Alloy (46% Ni). Alloy 46 was used because its coefficient of thermal expansion (7.5 ppm/°C) closely matched that of alumina (7.4 ppm/°C). The dimensions of the electrode rings (Figure 1a, computer aided design [CAD]) were 58.4 mm i.d., 66.7 mm o.d., and 8 mm wide. The electrode rings were machined to feature a small stepped face on each side (Figure 1b,c, front and back faces). The stepped face was created by a 0.5 × 0.9 mm (width × height) ridge extruding from either side of a 2 mm wide central rim. From either side of this 0.5 mm ridge, the electrode portion of the part extended another 2.5 mm. This stepped face served to maintain a face-to-face contact between adjacent rings while creating a cavity into which ceramic adhesive would be injected in a later step. By injecting ceramic adhesive in this manner, the known length of the drift tube was not altered by an unknown thickness of adhesive between rings; therefore, the rings remained parallel so that the homogeneity of the electric field was maintained. A 1.45 mm diameter (d) × 10 cm long threaded rod was screwed into a hole at the top of each electrode ring's central rim, which served as an electrode post and connection to the voltage divider through pin connectors (Positronic Industries, Inc.; Springfield, MO).

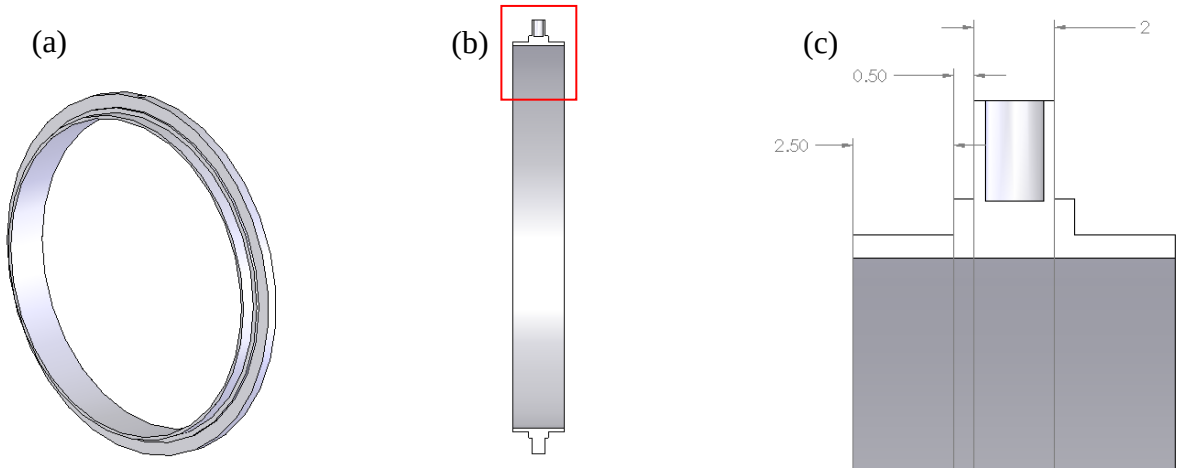

Figure 1. CAD drawings of (a) Alloy 46 electrode ring, (b) cross section of the Alloy 46 electrode ring, and (c) detailed view of the stepped face cross section that is highlighted by the red box in (b). Dimensions are in millimeters.

Figure 2a shows three electrodes and three insulator rings. When the ring portions of the electrodes were fitted within the inside diameter of the insulator rings, the faces of the insulator rings made contact with the faces of the 0.5 mm ridge on the electrode rings. This left a 0.5 mm wide cavity between the insulator ring and the face of the central rim on the electrode, as well as a distance of 3 mm between the insulator rings (Figure 2b). One electrode ring in the reaction and drift regions of the IMS instrument was specially machined to feature a hollow electrode post for the insertion of T100-250 temperature probes to enable the direct measurement of the drift gas temperature. A 1/8 in. Swagelok fitting (Swagelok; Solon, OH) was attached to the top of these hollow electrode posts to enable the pressure sealing of the ports.

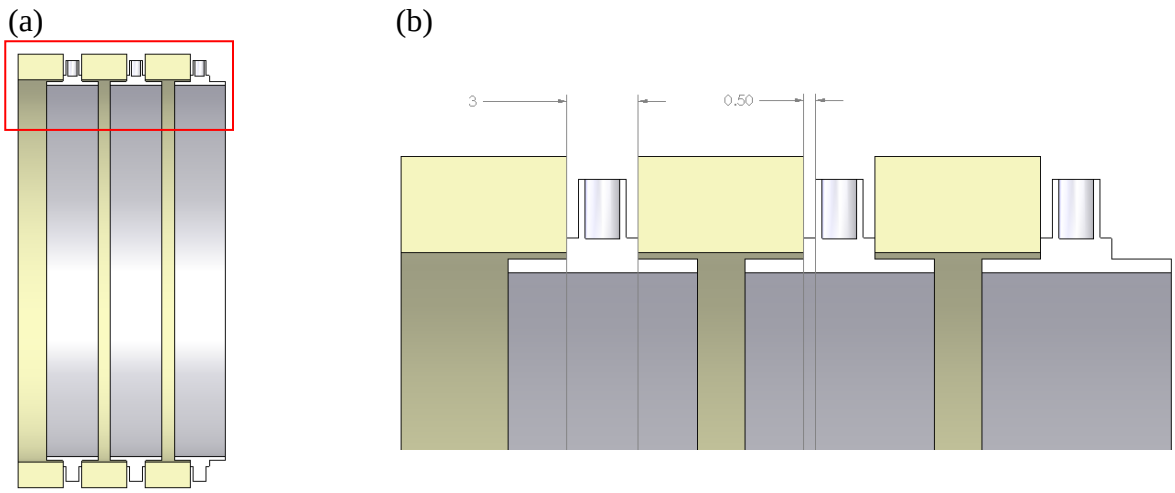

Figure 2. CAD drawings of (a) cross section of a stacked ring assembly consisting of three Alloy 46 electrodes (gray) and three ceramic insulator rings (tan) and (b) detailed view of the spacing of the drift rings that are highlighted by the red box shown in (a).

2.2.2 BN Ion Gates

The IMS drift tube contained two BN ion gates, which were used to initiate the drift time measurements. These gates were constructed using existing methods within the laboratory at WSU. Each BN ion gate consisted of a single ceramic insulator ring cut in half radially. A 1.27 mm wide channel was ground into the outer face of each half ring. One side of the channel was also ground down to 66.18 mm o.d. The smaller outside diameter faces of the two BN ion gate halves were then cemented together with an array of parallel 0.003 in. o.d. Alloy 46 wires (California Fine Wire Company) were spaced between them on 0.005 in. centers. Alternating wires were electrically connected to create two interleaved sets of parallel and electrically isolated wires.

2.2.3 Ni-63 Ionization Source

Ni-63 was used to ionize the sample. The ion source was constructed to maintain a hermetic seal and confine the equipotential lines of the drift field to the interior of the drift tube. The Ni-63 ionization source base and interface are shown in Figure 3a. The ion source base was made of Alloy 46 and had four ceramic rods mounted to it. A wire mesh screen and cup holding a Ni-63 foil was mounted to the other end of the rods using small stubs attached to the base and Ni-63 cup. This ion source base screwed into the ionization source interface and compressed an Alloy 718 C-seal (Jetseal, Inc.; Spokane, WA) for vacuum sealing. The ionization source interface sat against the front face and inside a piece of 43.5 mm long alumina tubing with the same outside and inside diameters as the alumina insulator rings. On the other side of this alumina piece was the first electrode ring of the IMS instrument; a wire mesh screen was spot-welded to its front. This screen served to shield the equipotential lines within the drift tube from the grounded base plate of the ionization source. This set up straight and vertical equipotential lines to keep the ions on a straight path towards the detector. The ion source base and the first

electrode were machined to create a 0.5 mm cavity (identical to the ones described in Figure 2b) between them and the long alumina piece. When the ion source base was screwed into the ion source interface, as shown in Figure 3b, the ceramic rods on the base pushed the screen attached to the Ni-63-containing cup against the screen of the first electrode. This created an electrical contact and supplied high voltage to the Ni-63 foil to induce ionization.

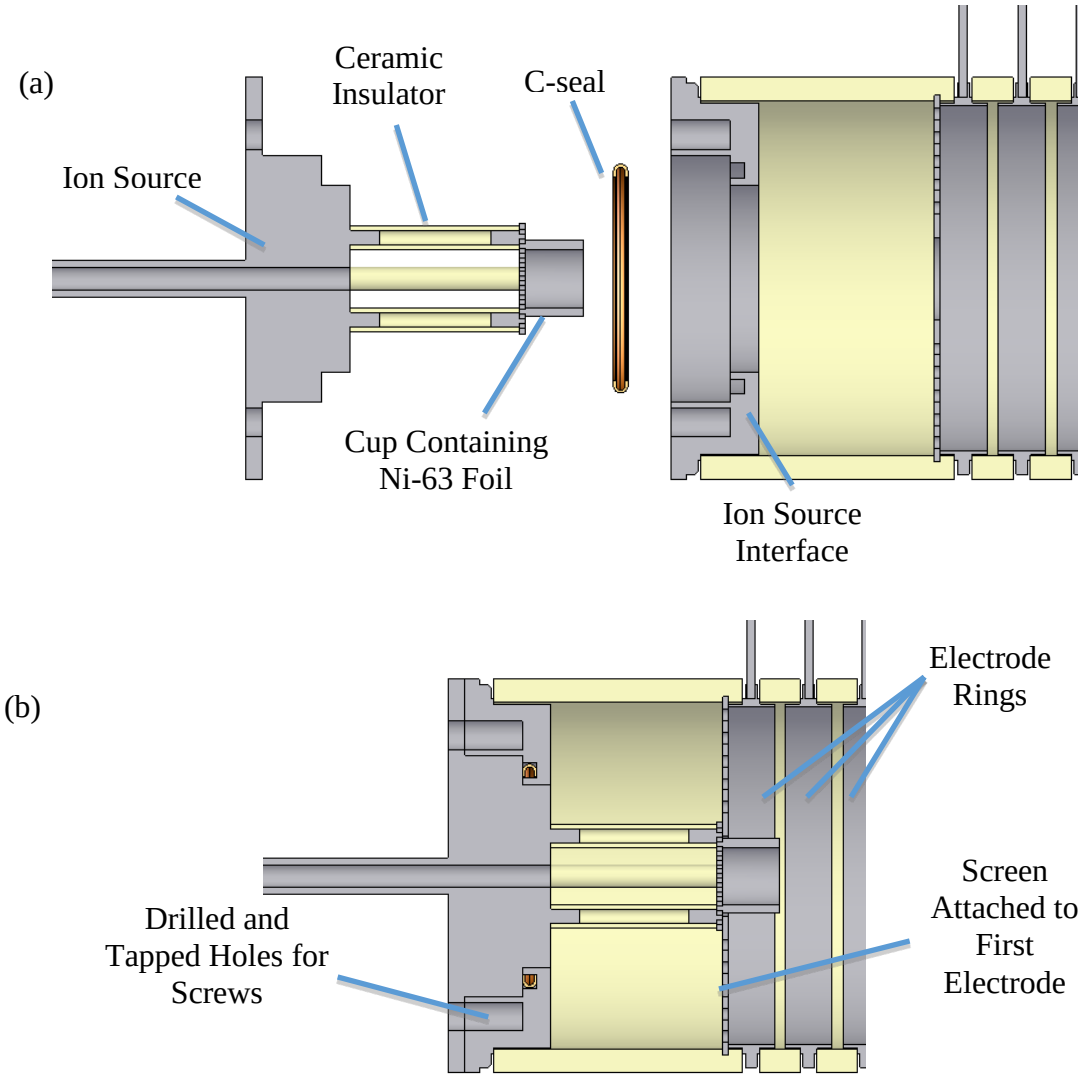

Figure 3. CAD drawing of the ionization source base, C-seal, and interface (a) separated and (b) joined together to make electrical contact between the Ni-63 cup and first electrode screen and to compress the C-seal between the ionization source base and interface.

2.2.4 Drift Gas Showerhead

The last electrode before the *tof*MS vacuum interface was used to introduce the neutral counter-current flow of drift gas. This electrode contained a Faraday plate for optional standalone analyses without the *tof*MS as the detector. The drift gas was introduced using a "showerhead" design. The drift gas showerhead/Faraday plate assembly, shown in Figure 4, was

placed behind the second gate and just before the pressure interface of the *tof*MS. It consisted of a central annular Faraday plate cemented within a piece of insulating alumina tubing using Resbond 920 fast-curing ceramic adhesive (Cotronics Corp.; Brooklyn, NY). The alumina tubing holding the Faraday plate was likewise cemented within the inside diameter of the drift gas entry showerhead. Three different leads were seated on top of the showerhead; the first was a metal-to-ceramic brazed isolator on the left (Solid Sealing Technology, Inc.; Watervliet, NY). This isolator was hollow. It allowed for the attachment of a drift gas line using 1/8 in. Swagelok fittings and kept the line electrically isolated from the voltage applied to the showerhead. The next two leads were placed on the right and were inline with one another along the axis of the drift tube. The lead in front was a BNC cable attached to a 1 kV feedthrough (Solid Sealing Technology). The other end of the feedthrough was spot-welded to the backside of the Faraday plate to complete the circuit for standalone Faraday plate analyses. The last lead behind the BNC cable lead was the threaded rod screwed into the showerhead to supply voltage. The outside diameter of the showerhead was the same as the ceramic insulator rings, and its front face was machined to create a 0.5 mm cavity (identical to the ones described in Figure 2b when placed against the second gate).

Figure 4. Front view of the drift gas showerhead assembly showing the Faraday plate and insulating ceramic cemented in the center, (left) the drift gas isolator, and (right) BNC signal lead on top of the showerhead base. The electrode post screwed into and supplying voltage to the base is in line behind the BNC signal lead.

2.2.5 Pressure-Sealing Procedure

2.2.5.1 Drift Ring Joints

To pressure seal each of the joints between the electrode and insulator rings, the two sections of the drift tube with continuous inside diameters (the drift region and reaction region, excluding the BN ion gates) were mounted separately onto an adjustable mandrel that was tightly clamped down onto the mounted stack. The mandrel was used to keep all drift rings in place during construction and to ensure that the electrode rings were concentric and parallel to maintain a homogenous electric field. Resbond 920 fast-curing ceramic adhesive was injected into the 0.5 mm cavities created by the machined ridges previously described. The ceramic adhesive was allowed to air dry for 24 h, and then, each region was taken off the mandrel and heat cured in an oven at 150 ºC for an additional 24 h. A light layer of Durapot 801 ceramic potting material (Cotronics), was then applied to the cured cement to help strengthen the joints. Similarly, the layer of Durapot 801 was allowed to air dry and then heat cured. After the Durapot 801 was heat cured, a layer of Celvaseal liquid vacuum leak sealant (Myers Vacuum; Kittanning, PA) was brushed onto the joints and allowed to air dry for 2 weeks.

After drying, each part was again placed in the oven to melt away excess Celvaseal sealant and cure any that had permeated into the micropores of the ceramic. The parts were then cleaned of excess Celvaseal sealant using dichloromethane and cotton tipped applicators. This left a layer of Celvaseal sealant cured within the micropores of the drift tube joints. A second layer of Durapot 801 was then applied to the dried layer of Celvaseal sealant to encase the vacuum seal layer. Special care was taken to ensure that the second layer of Durapot 801 did not extend past the outside diameter of the ceramic insulator rings. Parts that were unable to be mounted on the mandrel (the BN ion gates, showerhead, first electrode, and ionization source interface) were lined up within the rest of the assembly on the bench top and a 36 in. bar clamp was used to fasten the stack to the bench top. This ensured a tight mating of all faces and prevented the rings from separating when the ceramic cement was injected into the remaining joints. The same sealing procedure was then repeated for the remaining joints. The pressure seal was periodically tested during the construction process using a vacuum stage attached to a large rotary vane pump and an analog pressure gauge until the desired pressure was achieved.

2.2.5.2 Front and Back End of the Drift Tube

The front end of the drift tube was sealed by the 39.7 mm o.d. × 34.5 mm i.d. C-seal (Figure 5). The C-seal was compressed by screwing down the ion source front plate using eight socket cap screws. Four springs (McMaster-Carr Supply Company; Robbinsville, NJ), each with a force of 19 lb/ft, were mounted equidistantly around four of the screws on the ion source front plate and compressed between the ion source front plate and the front plate of the thermal case holding the IMS instrument assembly. These springs pushed the IMS instrument up against the front of the *tof*MS and compressed a 2.25 in. i.d. X-profile, double-sealing O-ring (McMaster-Carr) that was placed around a seating ridge on the back of the drift gas showerhead. This double sealing O-ring created a pressure seal between the back of the showerhead and the front of the *tof*MS vacuum interface. The entire assembly is depicted by the dimetric cross

section illustrated in the CAD drawing in Figure 5. The IMS instrument is shown housed within an insulating ceramic tube, which was in turn housed within the aluminum thermal case built in-house at WSU. The thermal case was attached to the *tof*MS vacuum interface using screws and thumb nuts.

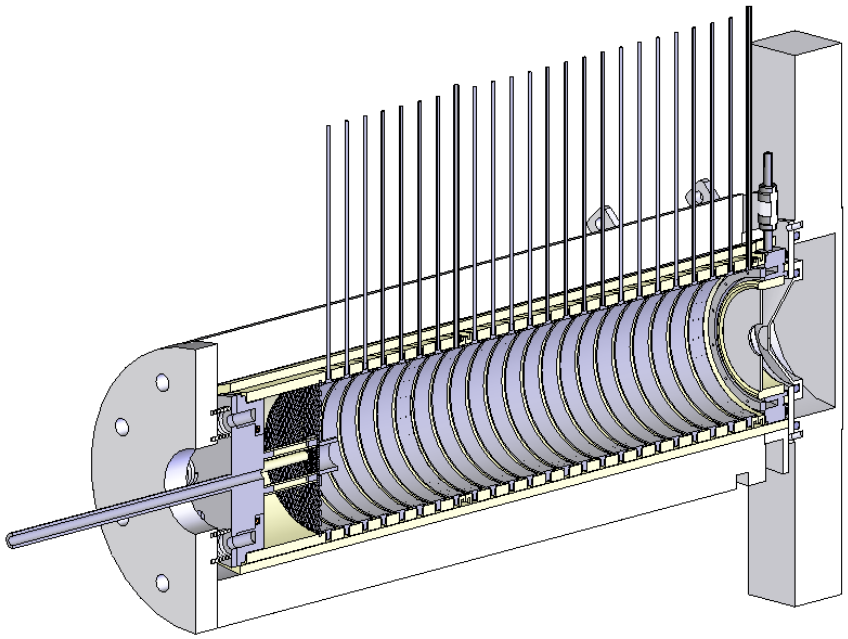

Figure 5. Dimetric cross section of constructed ion mobility spectrometer. Two hollow electrode posts before each gate allow for the insertion of temperature probes to directly measure the temperature of the drift gas and the introduction of sample through the first hollow electrode post.

2.2.5.3 Temperature Probe and Sample Entry Ports

The specialized electrode rings that allowed for the insertion of the temperature probes and sample needed to be pressure sealed but still be able to easily connect to the pin connectors of the resistor chain. This was done by modifying two fittings: a 1/8 in. Swagelok cap and an EZRU21 external/internal reducing union (Valco Instruments, Inc. Co.; Houston, TX), as shown in Figure 6. A small hole was drilled and tapped into each fitting (the inside diameter was not pierced), and a small piece of a threaded rod was screwed into the hole, onto which a male pin connector was soldered. The Valco external/internal reducing union was used on the electrode in the reaction region to allow for sample introduction into the drift tube through a silica capillary held by an FS1.36 fused silica adapter (Valco Instruments). The 1/8 in. Swagelok cap was used on the electrode ring in the drift region.

Figure 6. (Left) Modified Valco external/internal reducing union and (right) Swagelok cap used to make vacuum tight seals and provide easy electrical contact of the temperature probe drift rings to the resistor chain via the gold pin connectors soldered to the short posts drilled into the parts.

2.2.6 Ambient and Reduced Pressure Operation

Ambient pressure measurements were made by a mercury barometer, and the drift gas outlet was exposed to the laboratory atmosphere. Sub-ambient pressures were achieved by connecting the drift gas outlet to the 640A pressure controller and DS 42 rotary vane vacuum pump. The vacuum pump was turned on, and an orifice within the pressure controller restricted the flow of gas exiting the drift tube to establish the pressure set on the 247D power supply and readout.

2.2.7 Sample Introduction

Headspace vapor samples of volatile compounds were introduced into the instrument by placing 0.5 µL of neat sample in a 1/8 in. Swagelok cap and attaching the cap to the bottom of an 8 in. length of stainless steel tubing. The sample tee was connected with Swagelok fittings to a compressed air gas tank on one side and a 250 µm i.d. × 360 µm o.d. fused silica capillary through the Valco fittings on the other side. The capillary was inserted through the specialized temperature probe port and terminated in the reaction region in the center of the drift tube diameter. The capillary was held in place in the temperature probe port by the Valco fitting, which was adapted for electrical continuity. The orthogonal flow of gas carried the headspace vapors rising from the sample tee through the silica capillary and into the reaction region of the accurate IMS instrument. A 15 kV ceramic isolator (Solid Sealing Technology) ensured electrical isolation of the drift tube from the sample tee. Dimethyl methylphosphonate (DMMP) was the only volatile compound introduced in this manner for this study and was obtained as a 97% pure standard (Sigma Aldrich Chemical Co.; St. Louis, MO).

Nonvolatile compounds were introduced into the instrument by drawing an aliquot of the compound solution into a 17 cm silica capillary (150 µm i.d. × 360 µm o.d) using a 250 µL gastight number 1725 syringe (Hamilton Company; Reno, NV) and Valco fittings. The

solvent was allowed to evaporate for 1 h, which left solid explosives residue inside the capillary. The capillary was then attached to the sample line using external/internal reducing unions (Valco Instruments). The compressed air tank for the sample introduction line was then operated at 20 psi to carry the dichloromethane vapor (chloride dopant) and explosive sample vapor into the reaction region of the IMS instrument. When the temperature of the drift tube was not enough to volatilize the sample from inside the capillary, a secondary heat source was used. A 13.5 cm length of 1/16 in. o.d. alumina ceramic tubing (McMaster-Carr) was inserted into the temperature probe sample introduction port in the reaction region of the instrument so that 0.5 cm of tubing extended into the reaction region of the instrument and 2 cm of tubing extended out of the other end of the sample introduction port. Therefore, 11 cm of tubing was concealed within the inside diameter of the sample port tubing. An alumina fish spine bead was cemented to the outside diameter of the alumina tubing to prevent it from being pushed too far into the instrument. A 50 cm length of 90 Ω/ft resistance wire (Pelican Wire Company Inc.; Naples, FL) was then folded in half (care was taken not to damage the insulation), heat treated, and then inserted into the alumina tubing. The resistance wire was heat treated by connecting it to a Variac on the laboratory bench and slowly turning up the voltage to condition the wire to heat. The tip of the resistance wire was inserted 11 cm into the alumina tubing to terminate 0.5 cm from the end of the tubing. The alumina (ceramic) tubing was used to insulate the resistance wire from the high voltage of the drift tube. The ends of the resistance wire were then attached to a Variac. The sample capillary was inserted down into the alumina tubing, and explosives were volatilized from the capillary wall by operating the Variac at 25% full power to heat the resistance wire and capillary.

The explosives, 2,4,6-trinitrotoluene (TNT); 1,3,5-trinitroperhydro-1,3,5-triazine (RDX); and pentaerythritol tetranitrate (PETN), were introduced in this manner. These explosives were obtained as 5 mg/mL in methanol, 10 mg/mL in 1:1 methanol–acetonitrile, and 10 mg/mL in acetone, respectively, as stock solutions from AccuStandard (New Haven, CT). All stock solutions were diluted using high-performance liquid chromatography (HPLC)-grade methanol (Fisher Scientific International, Inc.; Waltham, MA) to create 0.1, 1, and 1 mg/mL solutions of TNT, RDX, and PETN, respectively.

2.2.8 Water Introduction

A 60 cm silica capillary (5 µm i.d. × 150 µm o.d.; Polymicro Technologies) was inserted into the drift gas line before the mass flow controller and connected on the other end to a 250 µL gastight number 1725 syringe through Valco fittings. A Fusion 200 syringe pump (Chemyx, Inc.; Stafford, TX) was operated at 0–85 µL/h (±<1%) at 20 µL/h intervals starting after 25 µL/h. An increase of 20 µL/h in the flow rate of the syringe pump resulted in approximately a 150–170 ppmv increase in the drift gas water content. After the water introduction junction, a Moisture Image Series 1 hygrometer and probe (GE Measurement and Control; Fairfield, CT) reported the water content of the drift gas. Labview software was used to record the values from the hygrometer every 10 s during the acquisition of each IM–*tof*MS spectrum. Other diameter capillaries and syringe pump flow rates may be used to achieve the desired drift gas water content levels. HPLC-grade water was obtained from Fisher Scientific.

2.2.9 Dopant Introduction

2.2.9.1 Positive Mode—Ammonia

A nominal concentration of 10 ppm ammonia was achieved using two permeation tubes (5.3 cm long and 0.64 cm o.d. each) that provided a combined permeation rate of 7065.04 ng/min with a flow of air at 1.000 ± 0.002 L/min and 23.4 ºC. The permeation tubes were inserted inline with the drift gas after the water introduction and before the hygrometer to verify that the ammonia solution did not increase the measured drift gas water content. The ammonia dopant was present in the drift and reaction regions of the IMS instrument. The calculated ammonia concentration at the nominal level of 10 ppm was 10.2 ppm at 23.4 °C. The positive-mode reactant ions changed from a series of hydronium water clusters to solely ammonium reactant ions in a series of water clusters. Ammonia was present in the drift gas in the positive- and negative-ion modes to simulate field instrument conditions.

2.2.9.2 Negative Mode—Dichloromethane

Dichloromethane (chloride) dopant was introduced into the IMS instrument simultaneously with the sample using a silica capillary (5 µm i.d. × 150 µm o.d.; Polymicro Technologies) that was inserted into the sample line upstream of the capillary containing the sample. The dichloromethane supply capillary was connected to a 250 µL gastight number 1725 syringe with Valco fittings. A Harvard Apparatus (Holliston, MA) Pump 11 Elite was operated at 0.06 µL/min (±0.01%) to introduce dichloromethane and shift the reactant ion chemistry to produce chloride as the dominant reactant ion. Chloride was present only in the negative ion mode and was only introduced with the sample (as opposed to with the drift gas) to simulate field instrument conditions. HPLC-grade dichloromethane was obtained from Fisher Scientific.

2.3 Assessment of Accuracy

Crawford et al. performed an error analysis on a stacked ring IMS-*tof*MS instrument with similar components to this instrument. They reported an accuracy of ±0.5%.[3] Improvements made when designing the current instrument, together with the procedures for the accurate and precise measurement[11] of the five variables in eq (1), improved the accuracy of K_0 value measurements to below ±0.2% (Table 1).

Table 1. Error Associated with each Variable when Calculating K_0 Values and the Source of Each Error at 50.21 ± 0.04 ºC and 280 V/cm on the Current Accurate IMS Instrument

Variable (units)	Error	Source of Largest Error
L (cm)	$S_L = \frac{0.007}{16.252} = 4 \times 10^{-4}$	Calipers
V (V)	$S_V = \frac{0.2}{4533.1} = 4 \times 10^{-5}$	High-voltage divider probe and digital multimeter
t_d (s)	$S_{t_d} = \frac{1 \times 10^{-9}}{1 \times 10^{-2}} = 1 \times 10^{-7}$	*tof*MS clock rate
T (K)	$S_T = \frac{0.04}{323.36} = 1 \times 10^{-4}$	Drift gas temperature gradient
P (Torr)	$S_P = \frac{0.2}{690} = 3 \times 10^{-4}$	Mercury barometer

Propagating the error associated with each variable in Table 1 through eq (1) produces an error of ±0.001 $cm^2V^{-1}s^{-1}$ for a K_0 value of 1 and ±0.002 $cm^2V^{-1}s^{-1}$ for a K_0 value of 2, which amounts to an optimal error of ±0.1% for obtained K_0 values. Improvements to the instrument design and procedures contributed to this improved error. The current accurate IMS instrument used the same measurement and control equipment for the five variables as the drift tube built by Crawford et al., except for the high-voltage power supplies, temperature controller, and the mass flow and pressure controllers. The first used high-voltage power supplies that had a 15 ppm output ripple, whereas the output ripple of the current high-voltage power supply was 1 ppm. This reduced the variability of the applied electric field strength. Design elements of the accurate IMS instrument also improved the accuracy. The electrodes within the stacked ring drift tube built by Crawford et al.[3] were not fixed in place but were stacked and held together under spring tension. The current accurate IMS instrument's electrodes and ceramic insulator rings were fixed in place and assembled in a concentric and parallel manner. This eliminated inhomogeneity within the electric field created by inconsistent stacking. The drift tube built by Crawford et al. only contained one BN ion gate, and their residence time within the *tof*MS was determined by plotting the t_d of the ion as a function of the inverse voltage drop, which has been shown to be a more inaccurate method.[12] Using two BN ion gates in the current accurate IMS instrument directly correlated the measured length to the t_d measurement. Crawford et al. were only able to reduce the drift gas temperature gradients between the BN ion gate and the *tof*MS vacuum interface inlet to within ±0.5 ºC. Instead, the method of preheating the drift gas in the current drift tube, in which a resistive wire heater was used, improved the drift gas temperature gradients between the BN ion gates by an order of magnitude to a maximum of ±0.05 ºC.[11] The pressure measurement taken from the mercury barometer was also corrected for temperature and gravity due to latitude, which was not done in the past.

2.4 Assessment of Hermetic Seal

Before the final assembly step, in which the separate drift tube sections were cemented together, the BN ion gates, the drift region, and the reaction region were separately tested for their use in maintaining an internal vacuum. Each BN ion gate was able to achieve an internal pressure of 0.01 Torr, and each of the drift and reaction regions was able to achieve an internal pressure of 0.02 Torr. Upon completion of the drift tube construction and its installation onto the *tof*MS, the DS42 vacuum pump was attached to the drift gas outlet but left in the off position, and the drift gas flow was also off. It was observed that the pinhole of the *tof*MS alone was able to evacuate the drift tube to 69 Torr. The pressures within the two-stage vacuum interface also decreased from 1.7 and 3.5×10^{-2} Torr to 3.0×10^{-1} and 9.9×10^{-3} Torr, respectively. When the vacuum pump was turned on (the drift gas flow was still off), the pressure within the drift tube further decreased to 10 Torr, and the *tof*MS interface pressures decreased to 8.0×10^{-2} and 6.4×10^{-3} Torr. This type of vacuum is more than sufficient to obtain desired pressures down to 0.5 atm to conduct pressure experiments as well as ensure the safe execution of experiments involving hazardous chemicals such as CWAs. The ability to conduct these sub-ambient experiments was further demonstrated when the mass flow and pressure controllers were able to achieve a drift gas flow rate measurement of 1 L/min and an internal pressure of 200 Torr, respectively.

The performance of the instrument was tested under reduced pressures by collecting DMMP spectra at 202 Torr. Figure 7 shows the reduced pressure spectrum compared with a spectrum taken at an ambient pressure of approximately 697 Torr. Both pressure conditions produced the same reactant and product ions, as shown in the *x* axis of Figure 7. The three drift time peaks corresponded to the proton-bound dimer of ammonia [$NH_3(NH_4)^+$, mass-to-charge ratio (*m/z*) 35]; the ammoniated monomer of DMMP [$DMMP(NH_4)^+$, *m/z* 142]; and the ammonium-bound dimer of DMMP [$(DMMP)_2(NH_4)^+$, *m/z* 266]. Each of these ions also fragmented in the *tof*MS vacuum interface into ammonium [NH_4^+, *m/z* 18]; the protonated monomer of DMMP [$DMMPH^+$, *m/z* 125]; and the proton-bound dimer of DMMP [$(DMMP)_2H^+$, *m/z* 249]. All three drift time peaks shifted to faster drift times and became sharper at 202 Torr. The resolution of the three peaks decreased as they shifted closer to one another. This demonstrates that the accurate IMS instrument can be hermetically sealed and is operational at reduced pressures. The instrument will allow for the analysis of hazardous chemicals such as active CWAs.

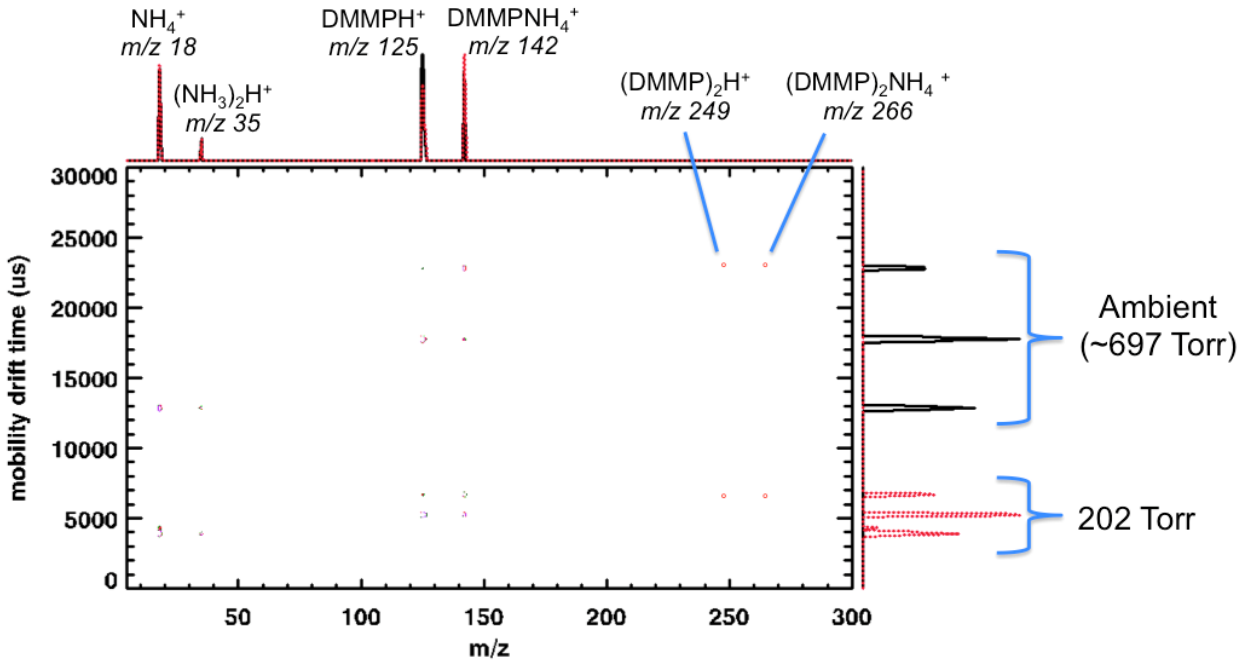

Figure 7. Overlay of DMMP spectra at ambient pressure (black trace) and reduced pressure (red trace). Both spectra were taken at 425 V/cm and the drift gas had a moisture content of <5 ppmv. As the pressure inside the IMS instrument was decreased, the drift time peaks shifted to faster drift times, higher resolution, and lower resolving power.

2.5 Initial Database of Accurate K_0 COI Values

The accurate K_0 values of the COIs (ammonia reactant ion, DMMP, TNT, RDX, and PETN) are shown in Tables 2–9. The compounds were analyzed as a function of temperature, drift gas water content, and electric field. The compounds were analyzed as a function of temperature and drift gas water content because it has been shown that K_0 values may change because of varying degrees of clustering reactions occurring within the drift tube. The response to these two variables was also investigated to potentially develop DMMP as an accurate mobility reference standard and empirically measure the drift gas water content using the ratio of monomer-to-dimer K_0 values.[10] The compounds were analyzed as a function of electric field because of a new breakthrough by Hauck et al., which illustrated the dependence of a K_0 value on low electric fields.[11,12]

Table 2. K_0 Values of $NH_3(NH_4)^+$, $DMMP(NH_4)^+$, and $(DMMP)_2(NH_4)^+$ at 280.2 V/cm as a Function of Drift Gas Water Content at Four Drift Gas Temperatures with the Electric Field Strength Held Constant

Average Drift Gas Temperature	**Average Drift Gas Water Content**	***K₀*** Value (precision, accuracy)		
°C	ppmv H_2O	$cm^2V^{-1}s^{-1}$		
		$NH_3(NH_4)^+$ *m/z* 35	$DMMP(NH_4)^+$ *m/z* 142	$(DMMP)_2(NH_4)^+$ *m/z* 266
26.18 ± 0.03	1.33 ± 0.01	2.328 (±0.002, ±0.002)	1.671 (±0.001, ±0.002)	1.323 (±0.002, ±0.002)
	166 ± 5	2.185 (±0.003, ±0.003)	1.645 (±0.002, ±0.002)	1.319 (±0.001, ±0.001)
	352 ± 5	2.125 (±0.001, ±0.002)	1.6280 (±0.0004, ±0.002)	1.317 (±0.001, ±0.001)
	509 ± 1	2.079 (±0.001, ±0.002)	1.615 (±0.001, ±0.002)	1.3132 (±0.0005, ±0.001)
	641 ± 3	2.056 (±0.001, ±0.002)	1.608 (±0.002, ±0.002)	1.312 (±0.002, ±0.002)
30.05 ± 0.01	1.632 ± 0.002	2.347 (±0.001, ±0.002)	1.676 (±0.001, ±0.002)	1.323 (±0.002, ±0.002)
	130 ± 16	2.217 (±0.002, ±0.002)	1.654 (±0.001, ±0.002)	1.320 (±0.001, ±0.001)
	257 ± 2	2.161 (±0.002, ±0.002)	1.640 (±0.001, ±0.002)	1.319 (±0.001, ±0.001)
	421 ± 2	2.111 (±0.001, ±0.002)	1.628 (±0.001, ±0.002)	1.316 (±0.001, ±0.001)
	580 ± 3	2.079 (±0.001, ±0.002)	1.617 (±0.001, ±0.002)	1.312 (±0.001, ±0.001)
40.15 ± 0.01	1.036 ± 0.007	2.386 (±0.002, ±0.002)	1.6926 (±0.0003, ±0.002)	1.323 (±0.001, ±0.001)
	144 ± 4	2.263 (±0.002, ±0.002)	1.671 (±0.002, ±0.002)	1.321 (±0.001, ±0.001)
	340 ± 4	2.199 (±0.004, ±0.004)	1.656 (±0.001, ±0.002)	1.320 (±0.001, ±0.001)
	452 ± 14	2.167 (±0.001, ±0.002)	1.648 (±0.002, ±0.002)	1.3192 (±0.0003, ±0.001)
	606 ± 2	2.1322 (±0.0002, ±0.002)	1.640 (±0.001, ±0.002)	1.317 (±0.001, ±0.001)
50.21 ± 0.04	1.494 ± 0.009	2.420 (±0.001, ±0.002)	1.7114 (±0.0002, ±0.002)	1.323 (±0.001, ±0.001)
	166 ± 2	2.298 (±0.001, ±0.002)	1.6873 (±0.0003, ±0.002)	1.320 (±0.001, ±0.001)
	342 ± 1	2.244 (±0.001, ±0.002)	1.675 (±0.001, ±0.002)	1.320 (±0.001, ±0.001)
	477 ± 1	2.2119 (±0.0003, ±0.002)	1.666 (±0.001, ±0.002)	1.319 (±0.001, ±0.001)
	621 ± 2	2.181 (±0.001, ±0.002)	1.6589 (±0.0003, ±0.002)	1.3176 (±0.0004, ±0.001)

Note: The precision followed by the accuracy of each data point is reported in parentheses.

Table 3. K_0 Ion Values of $NH_3(NH_4)^+$, $DMMP(NH_4)^+$, and $(DMMP)_2(NH_4)^+$ at 30.05 ± 0.01 °C as a Function of Drift Gas Water Content at Four Electric Field Strengths with the Drift Gas Temperature Held Constant

Electric Field Strength	**Average Drift Gas Water Content**	K_0 Value (precision, accuracy)		
		$cm^2V^{-1}s^{-1}$		
V/cm	ppmv H_2O	$NH_3(NH_4)^+$ *m/z* 35	$DMMP(NH_4)^+$ *m/z* 142	$(DMMP)_2(NH_4)^+$ *m/z* 266
280.2	1.632 ± 0.002	2.347 (±0.001, ±0.001)	1.676 (±0.001, ±0.002)	1.323 (±0.002, ±0.002)
	130 ± 16	2.217 (±0.002, ±0.002)	1.654 (±0.001, ±0.002)	1.320 (±0.001, ±0.001)
	257± 2	2.161 (±0.002, ±0.002)	1.640 (±0.001, ±0.002)	1.319 (±0.001, ±0.001)
	421 ± 2	2.111 (±0.001, ±0.001)	1.628 (±0.001, ±0.002)	1.316 (±0.001, ±0.001)
	580 ± 3	2.079 (±0.001, ±0.001)	1.617 (±0.001, ±0.002)	1.312 (±0.001, ±0.001)
350.1	0.899 ± 0.004	2.349 (±0.001, ±0.002)	1.6748 (±0.0004, ±0.002)	1.321 (±0.001, ±0.001)
	138 ± 13	2.209 (±0.006, ±0.006)	1.652 (±0.001, ±0.002)	1.3187 (±0.0002, ±0.001)
	216 ± 1	2.168 (±0.001, ±0.002)	1.640 (± 0.001, ±0.002)	1.317 (±0.001, ±0.001)
	380 ± 13	2.117 (±0.003, ±0.003)	1.627 (±0.001, ±0.002)	1.312 (±0.001, ±0.001)
	498 ± 4	2.086 (±0.001, ±0.002)	1.619 (±0.002, ±0.002)	1.311 (±0.001, ±0.001)
450.7	1.933 ± 0.004	2.341 (±0.001, ±0.002)	1.6715 (±0.0005, ±0.002)	1.319 (±0.001, ±0.001)
	151 ± 1	2.204 (±0.001, ±0.002)	1.647 (±0.001, ±0.002)	1.314 (±0.001, ±0.001)
	318 ± 2	2.146 (±0.002, ±0.002)	1.632 (±0.001, ±0.002)	1.313 (±0.001, ±0.001)
	437 ± 1	2.107 (±0.001, ±0.002)	1.622 (±0.001, ±0.002)	1.311 (±0.001, ±0.001)
	567 ± 2	2.076 (±0.001, ±0.002)	1.6131 (±0.0004, ±0.002)	1.308 (±0.001, ±0.001)
525.1	1.848 ± 0.002	2.339 (±0.001, ±0.002)	1.670 (±0.001, ±0.002)	1.319 (±0.002, ±0.002)
	145 ± 2	2.208 (±0.002, ±0.002)	1.647 (±0.001, ±0.002)	1.315 (±0.001, ±0.001)
	324 ± 5	2.1423 (±0.0005, ±0.002)	1.631 (±0.002, ±0.002)	1.3134 (±0.0005, ±0.001)
	479 ± 1	2.090 (±0.002, ±0.002)	1.617 (±0.001, ±0.002)	1.310 (±0.002, ±0.002)
	579 ± 1	2.071 (±0.001, ±0.002)	1.612 (±0.001, ±0.002)	1.3077 (±0.0005, ±0.001)

Note: The precision followed by the accuracy of each data point is reported in parentheses.

Table 4. K_0 Values of the Proton-Abstracted TNT Ion $(TNT\text{-}H)^-$ at 280.2 V/cm as a Function of Drift Gas Water Content at Four Drift Gas Temperatures with the Electric Field Strength Held Constant

Average Drift Gas Temperature	**Average Drift Gas Water Content**	***K₀*** Value (precision, accuracy)
		$cm^2V^{-1}s^{-1}$
°C	ppmv H_2O	$(TNT\text{-}H)^-$ *m/z* 226
26.18 ± 0.03	1.107 ± 0.004	1.568 (±0.002, ±0.002)
	173 ± 4	1.564 (±0.001, ±0.002)
	343 ± 1	1.564 (±0.001, ±0.002)
	507 ± 18	1.562 (±0.001, ±0.002)
	628 ± 6	1.558 (±0.001, ±0.002)
30.05 ± 0.01	0.887 ± 0.001	1.5679 (±0.0005, ±0.002)
	164 ± 3	1.566 (±0.001, ±0.002)
	339 ± 1	1.565 (±0.001, ±0.002)
	420 ± 12	1.563 (±0.002, ±0.002)
	630 ± 10	1.562 (±0.001, ±0.002)
40.15 ± 0.01	1.36 ± 0.02	1.5700 (±0.0002, ±0.002)
	160 ± 2	1.569 (±0.001, ±0.002)
	325 ± 2	1.567 (±0.001, ±0.002)
	472 ± 9	1.567 (±0.002, ±0.002)
	589 ± 12	1.5645 (±0.0004, ±0.002)
50.21 ± 0.04	0.840 ± 0.001	1.571 (±0.002, ±0.002)
	151 ± 4	1.5687 (±0.0003, ±0.002)
	312 ± 4	1.567 (±0.002, ±0.002)
	455 ± 9	1.566 (±0.001, ±0.002)
	568 ± 6	1.566 (±0.001, ±0.002)

Note: The precision followed by the accuracy of each data point is reported in parentheses.

Table 5. K_0 Values of $(TNT\text{-}H)^-$ at 30.05 ± 0.01 °C as a Function of Drift Gas Water Content at Four Electric Field Strengths with the Drift Gas Temperature Held Constant

Electric Field Strength	**Average Drift Gas Water Content**	***K₀*** Value (precision, accuracy)
V/cm	ppmv H_2O	$cm^2V^{-1}s^{-1}$ $(TNT\text{-}H)^-$ *m/z* 226
280.7	0.887 ± 0.001	1.5679 (±0.0005, ±0.002)
	164 ± 3	1.566 (±0.001, ±0.002)
	339 ± 1	1.565 (±0.001, ±0.002)
	420 ± 12	1.563 (±0.002, ±0.002)
	630 ± 10	1.562 (±0.001, ±0.002)
350.3	1.14 ± 0.02	1.5637 (±0.0004, ±0.002)
	185 ± 20	1.562 (±0.001, ±0.002)
	350 ± 6	1.561 (±0.002, ±0.002)
	472 ± 35	1.559 (±0.001, ±0.002)
	643 ± 31	1.560 (±0.001, ±0.002)
450.8	1.450 ± 0.008	1.560 (±0.001, ±0.002)
	172 ± 14	1.558 (±0.002, ±0.002)
	332 ± 1	1.556 (±0.001, ±0.002)
	455 ± 17	1.5567 (±0.0004, ±0.002)
	551 ± 4	1.556 (±0.001, ±0.002)
525.3	1.75 ± 0.01	1.560 (±0.001, ±0.002)
	176 ± 34	1.558 (±0.001, ±0.002)
	353 ± 12	1.558 (±0.001, ±0.002)
	519 ± 5	1.555 (±0.002, ±0.002)
	601 ± 11	1.553 (±0.001, ±0.002)

Note: The precision followed by the accuracy of each data point is reported in parentheses.

Table 6. K_0 Values of the RDX Chloride Adduct $(RDX+Cl)^-$ at 280.2 V/cm as a Function of Drift Gas Water Content at Four Drift Gas Temperatures

Average Drift Gas Temperature	**Average Drift Gas Water Content**	***K₀*** value (precision, accuracy)
°C	ppmv H_2O	$cm^2V^{-1}s^{-1}$ $(RDX+Cl)^-$ *m/z* 257
26.18 ± 0.03	1.680 ± 0.005	1.506 (±0.001, ±0.002)
	172 ± 38	1.476 (±0.001, ±0.002)
	340 ± 1	1.464 (±0.001, ±0.002)
	490 ± 8	1.452 (±0.002, ±0.002)
	601 ± 13	1.444 (±0.001, ±0.001)
30.05 ± 0.01	2.707 ± 0.004	1.5059 (±0.0003, ±0.002)
	176 ± 51	1.476 (±0.002, ±0.002)
	342 ± 9	1.461 (±0.001, ±0.002)
	493 ± 6	1.451 (±0.002, ±0.002)
	625 ± 9	1.444 (±0.002, ±0.002)
40.15 ± 0.01	1.31 ± 0.07	1.509 (±0.001, ±0.002)
	157 ± 9	1.488 (±0.002, ±0.002)
	277 ± 47	1.477 (±0.002, ±0.002)
	412 ± 1	1.470 (±0.002, ±0.002)
	589 ± 12	1.460 (±0.002, ±0.002)
50.21 ± 0.04	1.068 ± 0.004	1.5086 (±0.0004, ±0.002)
	147 ± 4	1.495 (±0.001, ±0.002)
	233 ± 2	1.4894 (±0.0002, ±0.002)
	312 ± 4	1.4845 (±0.0002, ±0.002)
	387 ± 3	1.479 (±0.002, ±0.002)
	457 ± 1	1.479 (±0.002, ±0.002)
	574 ± 9	1.472 (±0.001, ±0.002)

Note: The electric field strength was held constant and the precision followed by the accuracy of each data point is reported in parentheses.

Table 7. K_0 Values of $(RDX+Cl)^-$ at 30.05 ± 0.01 °C as a Function of Drift Gas Water Content at Four Electric Field Strengths

Electric Field Strength	**Average Drift Gas Water Content**	***K₀*** Value (precision, accuracy)
V/cm	ppmv H_2O	$cm^2V^{-1}s^{-1}$ $(RDX+Cl)^-$ *m/z* 257
280.6	2.707 ± 0.004	1.5059 (±0.0003, ±0.002)
	176 ± 51	1.476 (±0.002, ±0.002)
	342 ± 9	1.461 (±0.001, ±0.002)
	493 ± 6	1.451 (±0.002, ±0.002)
	625 ± 9	1.444 (±0.002, ±0.002)
350.0	2.80 ± 0.01	1.502 (±0.001, ±0.002)
	180 ± 51	1.472 (±0.002, ±0.002)
	332 ± 3	1.460 (±0.001, ±0.002)
	461 ± 12	1.450 (±0.002, ±0.002)
	585 ± 13	1.443 (±0.001, ±0.001)
450.2	1.463 ± 0.003	1.499 (±0.001, ±0.002)
	171 ± 32	1.463 (±0.002, ±0.002)
	338 ± 7	1.444 (±0.002, ±0.001)
	481 ± 8	1.440 (±0.001, ±0.001)
	643 ± 7	1.432 (±0.002, ±0.001)
525.0	2.983 ± 0.004	1.499 (±0.001, ±0.002)
	176 ± 46	1.468 (±0.002, ±0.002)
	340 ± 5	1.455 (±0.001, ±0.002)
	485 ± 1	1.447 (±0.001, ±0.002)
	632 ± 16	1.437 (±0.001, ±0.001)

Note: The electric field strength was held constant and the precision followed by the accuracy of each data point is reported in parentheses.

Table 8. K_0 Values of the PETN Chloride Adduct $(PETN+Cl)^-$ at 280.2 V/cm as a Function of Drift Gas Water Content at Four Drift Gas Temperatures

Average Drift Gas Temperature	**Average Drift Gas Water Content**	***K₀*** Value (precision, accuracy)
°C	ppmv H_2O	$cm^2V^{-1}s^{-1}$
		$(PETN+Cl)^-$ *m/z* 351
26.18 ± 0.03	1.436 ± 0.004	1.260 (±0.001, ±0.001)
	159 ± 2	1.241 (±0.002, ±0.002)
	321 ± 4	1.235 (±0.001, ±0.001)
	444 ± 3	1.232 (±0.001, ±0.001)
	608 ± 37	1.223 (±0.002, ±0.002)
30.05 ± 0.01	1.754 ± 0.004	1.261 (±0.001, ±0.001)
	155 ± 3	1.240 (±0.001, ±0.001)
	317 ± 2	1.231 (±0.002, ±0.002)
	449 ± 2	1.227 (±0.001, ±0.001)
	576 ± 14	1.2218 (±0.0005, ±0.001)
40.15 ± 0.01	1.36 ± 0.02	1.2611 (±0.0001, ±0.001)
	162 ± 1	1.249 (±0.001, ±0.001)
	323 ± 6	1.2406 (±0.0002, ±0.001)
	438 ± 20	1.236 (±0.001, ±0.001)
	542 ± 3	1.234 (±0.002, ±0.002)
50.21 ± 0.04	0.840 ± 0.001	1.262 (±0.001, ±0.001)
	151 ± 4	1.250 (±0.001, ±0.001)
	312 ± 4	1.2426 (±0.0002, ±0.001)
	455 ± 9	1.237 (±0.002, ±0.002)
	568 ± 6	1.233 (±0.001, ±0.001)

Note: The electric field strength was held constant and the precision followed by the accuracy of each data point is reported in parentheses.

Table 9. K_0 Values of $(PETN+Cl)^-$ at 30.05 ± 0.01 °C as a Function of Drift Gas Water Content at Four Electric Field Strengths

Electric Field Strength	**Average Drift Gas Water Content**	***K₀*** value (precision, accuracy)
V/cm	ppmv H_2O	$cm^2V^{-1}s^{-1}$ $(PETN+Cl)^-$ *m/z* 351
280.8	1.754 ± 0.004	1.261 (±0.001, ±0.001)
	155 ± 3	1.240 (±0.001, ±0.001)
	317 ± 2	1.231 (±0.002, ±0.002)
	449 ± 2	1.227 (±0.001, ±0.001)
	576 ± 14	1.2218 (±0.0005, ±0.001)
350.1	2.74 ± 0.03	1.258 (±0.001, ±0.001)
	171 ± 2	1.233 (±0.001, ±0.001)
	329 ± 6	1.2294 (±0.0003, ±0.001)
	462 ± 3	1.221 (±0.001, ±0.001)
	616 ± 3	1.218 (±0.002, ±0.002)
450.6	1.73 ± 0.03	1.258 (±0.001, ±0.001)
	166 ± 37	1.233 (±0.001, ±0.001)
	326 ± 1	1.225 (±0.001, ±0.001)
	465 ± 38	1.218 (±0.002, ±0.002)
	602 ± 4	1.214 (±0.001, ±0.001)
524.9	2.75 ± 0.01	1.256 (±0.001, ±0.001)
	177 ± 57	1.236 (±0.001, ±0.001)
	333 ± 29	1.223 (±0.001, ±0.001)
	465 ± 17	1.221 (±0.001, ±0.001)
	609 ± 32	1.216 (±0.002, ±0.002)

Note: The electric field strength was held constant and the precision followed by the accuracy of each data point is reported in parentheses.

3. FUTURE DIRECTIONS AND CONCLUSIONS

The accurate IMS–*tof*MS instrument described in this report was successfully delivered to ECBC for permanent installation. Using the data reported here and any data collected in the future, a database of accurate K_0 values will be developed for COIs. The reported K_0 values are accurate to ±0.2% or better. This is more than an order of magnitude improvement over previously reported accuracies for K_0 measurements.[3] Future work includes the evaluation of potential mobility reference standards to determine the best ones for use in the calibration process.

The data collected using this instrument will be used to create an improved detection algorithm for IMS-based field instruments. The rate of false-positive alarms on IMS-based field instruments will decrease through the use of these accurate K_0 values by propagating a lower degree of error when establishing detection windows. The instrument will still be able to maintain a low rate of false-negative responses by first using a correction factor to shift the mobility scale to the proper position based on the initial uncalibrated response of the instrument and the correct K_0 values of ions that are required to be used. The algorithm will be used to determine the correct K_0 values for the mobility reference standard and COIs using a matrix of values that are similar to the ones reported here and incorporate the operating parameters of the instrument. Therefore, the IMS-based field instrument will require only software changes and no hardware changes for improvement purposes.

LITERATURE CITED

1. Eiceman, G.A.; Karpas, Z.; Hill, H.H., Jr. *Ion Mobility Spectrometry*, 3rd ed.; CRC Press: Boca Raton, FL, 2014.

2. Kanu, A.B.; Haigh, P.E.; Hill, H.H., Jr. Surface Detection of Chemical Warfare Agent Simulants and Degradation Products. *Anal. Chim. Acta* **2005,** *553,* 148–159.

3. Crawford, C.L.; Hauck, B.C.; Tufariello, J.A.; Harden, C.S.; McHugh, V.; Siems, W. F.; Hill, H.H., Jr. Accurate and Reproducible Ion Mobility Measurements for Chemical Standard Evaluation. *Talanta* **2012,** *101,* 161–170.

4. Fernández-Maestre, R.; Harden, C.S.; Ewing, R.G.; Crawford, C.L.; Hill, H.H., Jr. Chemical Standards in Ion Mobility Spectrometry. *Analyst* **2010,** *135,* 1433–1442.

5. Eiceman, G.A.; Nazarov, E.G.; Stone, J.A. Chemical Standards in Ion Mobility Spectrometry. *Anal. Chim. Acta* **2003,** *493,* 185–194.

6. Ochoa, M.L.; Harrington, P.B. Detection of Methamphetamine in the Presence of Nicotine Using In Situ Chemical Derivatization and Ion Mobility Spectrometry. *Anal. Chem.* **2004,** *76,* 985–91.

7. Rearden, P.; Harrington, P.B. Rapid Screening of Precursor and Degradation Products of Chemical Warfare Agents in Soil by Solid-Phase Microextraction Ion Mobility Spectrometry (SPME-IMS). *Anal. Chim. Acta* **2005,** *545,* 13–20.

8. Kaur-Atwal, G.; O'Connor, G.; Aksenov, A.A.; Bocos-Bintintan, V.; Thomas, C.P.; Creaser, C.S. Chemical Standards for Ion Mobility Spectrometry: A Review. *Int. J. Ion Mobil. Spec.* **2009,** *12,* 1–14.

9. Clemmer, D.E.; Jarrold, M.F. Ion Mobility Measurements and their Applications to Clusters and Biomolecules. *J. Mass Spectrom.* **1997,** *32,* 577–592.

10. Hauck, B.C.; Davis, E.J.; Clark, A.E.; Siems, W.F.; Harden, C.S.; McHugh, V.M.; Hill, H.H., Jr. Determining the Water Content of a Drift Gas Using Reduced Ion Mobility Measurements. *Int. J. Mass Spectrom.* **2014,** *368,* 37–44.

11. Hauck, B.C.; Siems, W.F.; Harden, C.S.; McHugh, V.M.; Hill, H.H., Jr. *E/N* Effects on K_0 Values Revealed by High Precision Measurements Under Low Field Conditions. *Rev. Sci. Instrum.* **2016**B**,** *87,* 075104.

12. Hauck, B.C.; Siems, W.F.; Harden, C.S.; McHugh, V.M.; Hill, H.H., Jr. Determination of E/N Influence on K_0 Values within the Low Field Region of Ion Mobility Spectrometry. *J. Phys. Chem. A* **2017,** *121,* 2274–2281.

13 Hauck, B.C. High Accuracy Ion Mobility Spectrometry to Reduce False Alarm Rates in National Security Technology. Ph.D. Thesis, Washington State University, 2016.

14. Davis, E.J.; Clowers, B.H.; Siems, W.F.; Hill, H.H., Jr. Comprehensive Software Suite for the Operation, Maintenance, and Evaluation of an Ion Mobility Spectrometer. *Int. J. Ion Mobil. Spec.* **2011,** *14,* 117–124.

.

ACRONYMS AND ABBREVIATIONS

BN	Bradbury–Nielson
CAD	computer aided design
C_i	instrument factor
COI	compound of interest
CWA	chemical warfare agent
d	diameter
DMM	digital multimeter
DMMP	dimethyl methylphosphonate
$(DMMP)_2H^+$	proton-bound dimer of DMMP
$DMMP(NH_4)^+$	ammoniated monomer of DMMP
$(DMMP)_2(NH_4)^+$	ammonium-bound dimer of DMMP
$DMMPH^+$	protonated monomer of DMMP
E	electric field
ECBC	U.S. Army Edgewood Chemical Biological Center
HPLC	high-performance liquid chromatography
HV	high voltage
IIR	parallel resistance between measurement point and ground
IMS	ion mobility spectrometry
i.d.	inside diameter
K_0	reduced mobility
$K_{0\ COI}$	K_0 value of a compound of interest
$K_{0\ std}$	K_0 value of a mobility reference standard
L	length
$NH_3(NH_4)^+$	proton-bound dimer of ammonia
NH_4^+	ammonium
o.d.	outside diameter
P	pressure
PDR	probe divider ratio
PETN	pentaerythritol tetranitrate
$(PETN+Cl)^-$	chloride adduct of PETN
R_{dwnfld}	resistance downfield from measurement point
RDX	1,3,5-trinitroperhydro-1,3,5-triazine
$(RDX+Cl)^-$	chloride adduct of RDX
R_T	total resistance
RTD	resistive temperature device
R_{upfld}	resistance upfield from measurement point
T	temperature
t_d	drift time
$t_{d\ COI}$	drift time of a compound of interest
$t_{d\ std}$	drift time of a mobility reference standard
TNT	2,4,6-trinitrotoluene
$(TNT-H)^-$	Proton-abstracted ion of TNT
*tof*MS	time-of-flight mass spectrometer

V	voltage
V_{meas}	measured voltage
V_s	voltage applied to the first electrode ring
V_{true}	true voltage at measurement point
WSU	Washington State University

DISTRIBUTION LIST

The following individuals and organizations were provided with one Adobe portable document format (pdf) electronic version of this report:

U.S. Army Edgewood Chemical
Biological Center (ECBC)
RDCB-DRI-D
ATTN: McHugh, V.
Wade, M.

Defense Threat Reduction Agency
J9-CBS
ATTN: Graziano, A.

Department of Homeland Security
RDCB-PI-CSAC
ATTN: Negron, A.
DHS-S&T-RDP-CSAC
ATTN: Strang, P.

G-3 History Office
U.S. Army RDECOM
ATTN: Smart, J.

ECBC Technical Library
RDCB-DRB-BL
ATTN: Foppiano, S.
Stein, J.

Office of the Chief Counsel
AMSRD-CC
ATTN: Upchurch, V.

Defense Technical Information Center
ATTN: DTIC OA

ECBC Rock Island
RDCB-DES
ATTN: Lee, K.
RDCB-DEM
ATTN: Grodecki, J.


EDGEWOOD CHEMICAL BIOLOGICAL CENTER
A U.S. Army RDECOM Laboratory